ELSEVIER

Contents lists available at ScienceDirect

Construction and Building Materials

journal homepage: www.elsevier.com/locate/conbuildmat





Effects of magnesia in semi-hydraulic and non-hydraulic calcium silicate binders during carbonation curing

Rakibul I. Khan a,b, Salman Siddique , Warda Ashraf a,*

- a Department of Civil Engineering, University of Texas at Arlington, Nedderman Hall, Arlington, TX 76010, USA
- ^b Chemist II, Laticrete International, Inc., Bethany, CT 06524-3423, USA

ARTICLE INFO

Keywords:
Slag
Wollastonite
Magnesia
Carbonation
MgCO₃, CaCO₃, hydromagnesite, nesquehonite

ABSTRACT

This study presented an insight into the mechanical and microstructural properties of carbonated composites produced using slag, wollastonite, and magnesia. Paste batches containing various dosages of slag, wollastonite, and magnesia were subjected to carbonation curing regime at a concentration of 20% CO₂, 50 °C temperature, and 80% relative humidity. The microstructure of the samples was evaluated using scanning electron microscopy (SEM), dynamic vapor sorption (DVS), thermogravimetric analysis (TGA) coupled with mass spectroscopy (MS), Fourier transformed infrared spectroscopy (FTIR), and X-ray diffraction (XRD). It was observed that the formation of hydrated magnesium carbonates (HMCs) i.e., needle shape nesquehonite, Rosset-like hydromagnesite have increased the carbonated matrix density due to its expansive nature and by forming an interconnected network. The change in total and critical pore size distribution was observed with the addition of magnesia. The compressive strengths were also observed to increase by 44% and 126% when 25% magnesia was incorporated into wollastonite and slag composites, respectively. Furthermore, it was observed that under carbonation curing non-hydraulic wollastonite system performed better when compared to semi-hydraulic slag system.

1. Introduction

Ground granulated blast furnace slag (hereby referred as slag) have attracted attention due to latent hydraulic properties and its widespread availability. Furthermore, slag based cement composites have shown superior durability as represented by good resistance against chemical attacks, including chloride penetration [1-3]. On the other hand, wollastonite is a naturally occurring mineral which can be grounded into fine powder. Similar to slag, wollastonite (CaSiO₃) with its unique chemical and physical properties is also gaining recognition as potential cementitious material under carbonation curing [4-8]. Magnesia cement (hereby referred as magnesia) due to its relatively lower calcination temperature (650-800 °C) has been identified as a green cement [9–12]. Moreover, the CO₂ sequestration capacity of magnesia has also been recognized as a potential application sector [11,13-16]. Few studies have shown that incorporating magnesia in slag improves the hydration reaction and increases the CO₂ sequestration [3,17,18]. The increasing amount of magnesia in slag increases the formation of C-S-H gel in the hydrated system and increases the compressive strength [19].

Carbonation curing is a different curing system where prepared samples are kept in a CO₂-rich environment. During this carbonation

curing process, Ca and Si-rich materials will react with CO_2 in the presence of moisture and produce $CaCO_3$ and Ca-modified silica gel. Those two reaction products are the main binding phases in this curing system. This study investigated the effects of magnesia in slag and wollastonite systems under CO_2 curing through numerous techniques.

The carbonation of magnesia is also another way to strengthen the matrix. Carbonation is preceded by hydration, during which the dissolution of magnesia is associated with an increase in the pH of the pore solution, which promotes the dissolution of CO2 for the subsequent carbonation process. The dissolved CO2 reacts with Mg(OH)2 to form hydrated magnesium carbonates (HMCs) during carbonation. The formation of HMCs is associated with their expansive formation that reduces the porosity and establishes an interconnected network to provide binding ability, thereby strength gain of these binders. The most common HMCs in carbonated MgO are rosette-like hydro-magnesite (Mg₅(CO₃)₄.(OH)₂·4H₂O)), needle-like nesquehonite (MgCO₃·3H₂O), and dypingite (Mg₅(CO₃)0.4(OH)₂·5H₂O)) [20]. Several studies were performed on the carbonation of MgO and its effects on mechanical and microstructural performances [21-25]. Unluer and Al-Tabbaa used carbonation curing of reactive MgO to produce porous blocks [13]. It was reported that even 5% CO₂ curing for 24 h was sufficient to achieve

^{*} Corresponding author at: Department of Civil Engineering, University of Texas at Arlington, Nedderman Hall 417, 416 Yates Street, Arlington, TX 76010, USA. *E-mail address*: warda.ashraf@uta.edu (W. Ashraf).

the required strength of cement blocks. Zhang et al. developed a carbonated binder system containing Portland cement and reactive MgO [14]. The authors concluded that nesquehonite is formed only when MgO content is higher than 60% [14]. For a hydrated binder system containing around 50% MgO, hydrated Mg carbonate was formed. Wu et al. produced a carbonation cured composite containing reactive MgO and fly ash [26]. The carbonation curing for 1 day was deemed sufficient to enhance the engineering properties of composites containing 50% fly ash. Marmol et al. reported that using cellulose pulp in reactive MgO mix under carbonation curing enhances the formation of nesquehonite, which reduces the porosity of the mix [20]. Wang et al. used Portland cement and reactive MgO to develop a binary binder under carbonation curing [27]. It was reported that up to 29% gain in compressive strength can be achieved by curing at 10% CO₂ concentration for 7 days [27].

The present study focuses on the comparative analysis between the effects of magnesia in the semi-hydraulic system, i.e., slag, and non-hydraulic system, i.e., wollastonite, to determine the effects of magnesia in carbonates formations and CO₂ sequestration in both semi-hydraulic and non-hydraulic cementitious systems. Furthermore, comparison between slag (semi-hydraulic) system and wollastonite (non-hydraulic) was selected to draw proper understanding on how carbonation and incorporation of magnesia affects the physical properties of final product. The objectives of this study are to investigate: (i) the formation of carbonated products in the presence of magnesia, (ii) the effects of pore size distribution, and (iii) mechanical performances.

2. Materials and methods

2.1. Materials

Mortar and paste samples were prepared using ground granulated blast furnace slag (referred to as "slag"), wollastonite (CaSiO₃), magnesia (MgO), and ASTM standard sand. Cemex (CA, USA) provided the slag, while Nico Minerals (NY, USA) provided the wollastonite. MgO was purchased from VWR. Table 1 summarizes the chemical composition of slag and wollastonite.

2.2. Sample preparation

Two types of samples (i.e., paste and mortar) were prepared for this study. For mechanical performance and length change measurements, mortar samples were prepared using water to binder ratio of 0.60. The higher water to binder ratio was considered to produce workable mix. Furthermore, no treatment was carried out to the samples as they were immediately moved to carbonation curing after casting. For microstructural investigation, disk samples were prepared using paste mixes with the same water to binder ratio as considered for mortar mixes.

Seven sample batches were prepared for evaluation. These batches are 100% slag, 100% magnesia, 100% wollastonite, 75% slag-25% magnesia, 50% slag-50% magnesia, 75% wollastonite-25% magnesia, and 50% wollastonite-50% magnesia. The content of magnesia was fixed at 50% as higher amount of magnesia results in formation of expansive nesquehonite. First, powdered samples were dry mixed for 30 s and then combined with water at a ratio of 0.60 w/b for all batches, and then mixed for an additional 2 min at 400 rpm using a 'Renfert Twister Evolution mixer.' After mixing, the paste samples were put on a 20 mm disk molds. Immediately after casting, those disk samples were stored in a commercially available "VWR air jacket CO2 incubator" where 80% RH, 20% CO2 concentration, and 50 °C environment was maintained.

Higher relative humidity provides the required moisture in the carbonation reaction [3,17,28,29], and for wollastonite carbonation minimum of 50 $^{\circ}$ C is needed for the reaction to happen [5,6,30–32]. The disks were demolded after 24 h of casting and were again placed in the CO₂ incubator for further carbonation curing. The samples were collected after 14, 28, and 56 days and soaked in isopropanol for 24 h before being kept in a vacuum desiccator for 36 h to avoid further hydration/carbonation reactions. The samples were then investigated by various techniques to check for microstructural changes.

For mortar samples, binders were mixed with the water for 2 min at a speed of 140 revolutions/min in a commercially available Hobart rotatory mixture. The ASTM standard sand was added, and the mixing was maintained for another 1 min. Following a 30-second rest, the samples were mixed for 1 min at a speed of 285 revolutions/min. The combined mortar samples were used to cast 25 mm \times 25 mm \times 285 mm prisms and 50 mm cubes. Immediately after casting, the prism and beam samples were exposed to CO_2 environment. The carbonation environment was identical to that of paste samples. Similar to paste samples, after 24 h of carbonation, the mortar samples were demolded and carbonated in the same environment as before. Compressive strength tests were performed on cube samples obtained from the carbonation chamber after 14, 28, and 56 days. Table 2 includes details on the sample mixes and tests carried out in this study.

2.3. Test methods

2.3.1. Mechanical performances

The compressive strength of 50 mm cube was measured after 14, 28, and 56 days of carbonation curing. The compressive strength was measured via the MTS Landmark servo-hydraulic test system using a displacement rate of $0.02 \, \text{mm/sec}$.

2.3.2. Length change

The length change was measured according to the ASTM C157 standard [33]. Mortar prisms of dimensions $25 \text{ mm} \times 25 \text{ mm} \times 285 \text{ mm}$ prism were produced. Following the standard, those prisms were prepared into three layers. Immediately after casting, the samples were placed inside the carbonation chamber with the mold. After 48 h, the samples were demolded, and the length changes were monitored for 50 days. The length changes were calculated using the following equation in accordance with ASTM C157 [33].

Table 2Mix details of the samples.

Sample Name	Binders	;	Standard		
	Slag (%)	Wollastonite (%)	Magnesia (%)	sand/binder	
Slag	100	0	0	2.75	
Wollastonite	0	100	0	2.75	
Magnesia	0	0	100	2.75	
75% wollastonite- 25% magnesia	0	75	25	2.75	
75% slag-25% magnesia	75	0	25	2.75	
50% wollastonite- 50% magnesia	0	50	50	2.75	
50% slag-50% magnesia	50	0	50	2.75	

Table 1 Composition of slag and wollastonite.

	SiO_2	CaO	Al_2O_3	Fe_2O_3	MgO	SO_3	MnO	${\rm TiO_2}$
Slag (weight %)	29.6	36.4	15.6	0.37	9.69	5.19	0.49	1.47
Wollastonite (weight %)	55.0	43.6	0.463	0.261	0.457	0.05	0.04	0.01

Length chaage (%) =
$$\frac{CRD_f - CRD_i}{250} \times 100$$
 (1)

where CRD = difference between the comparator reading of the specimen and the reference bar at any age.

2.3.3. Thermogravimetric analysis (TGA)

A commercially available instrument (TA instrument, TGA 550) was used for the TGA experiment. The paste samples were collected from the disk samples in section 2.2. The collected samples were ground using a mortar pestle to obtain a fine powder. Approximately 35 mg of powdered sample was loaded into the platinum pan and kept under isothermal conditions for 5 min at 25 $^{\circ}$ C. The chamber temperature was then raised until 980 $^{\circ}$ C with an increment of 15 $^{\circ}$ C per minute. Nitrogen gas was purged to ensure an inert environment. Initially, three replicate samples were tested through TGA for a few batches to validate for any deviation in carbonation across samples. The test result deviations were less than 2% by weight of total carbonated samples. Due to the low variation, TGA was performed only with one sample for the remainder of the batches.

2.3.4. Thermogravimetric analysis with mass spectroscopy (TGA-MS)

For a few sample analysis, TGA coupled with a mass spectrometer (MS) was used. This coupled TGA-MS system enabled the separation and identification of any volatile elements coming off the sample during the heating process. In this case, TGA was performed using a Netzsch STA 449 F3 Jupiter Simultaneous Thermal Analysis (STA) instrument. All samples were measured under ultra-high purity helium gas (flow of 50 ml/min). The temperature was increased at a rate of 10 °C/min, and gases were transferred to the GC/MS instrumentation via a heated (250 °C) transfer line. An Agilent Technologies 7890A GC system equipped with a non-polar capillary column (Agilent J&B HP-5 packed with [5%-Phenyl-methylpolysiloxane]) coupled with a 5975 MSD spectrometer was used for the analyses of the gases released from the samples. A gas injection was triggered every minute (60 sec) from the beginning of the heating cycle, and 0.25 ml of gas was sampled from the gases released by the compound and carrier gas (He).

2.3.5. Fourier transformed infrared (FTIR)

The powered disk samples were used for FTIR measurement. The commercially available Nicolet iS50 FTIR from Thermo Scientific was used for this test. The spectra were collected using the Attenuated Total Reflection (ATR) mode with $4~{\rm cm}^{-1}$ resolution and 32 scans per sample.

2.3.6. X-ray diffraction (XRD)

X-ray diffraction patterns of samples were collected via Bruker D-500 spectrometer using a Cu K α radiation (40 kV, 30 mA). The diffraction patterns were obtained for the 2θ range of 5° to 80° using a step size of 0.02 (2 θ) per second.

XRD analysis was performed using commercially available software (Match! Phase Analysis using Powder Diffraction). The used PDF card numbers were PDF #96-900-1298, PDF #96-901-5894, PDF #96-900-2349, PDF #96-900-7621, PDF #96-901-2402, PDF #96-900-2821, PDF #96-101-1118, and PDF #96-900-5779 for calcite, aragonite, brucite, hydro-magnesite, nesquehonite, magnesite, MgO, and wollastonite respectively.

2.3.7. Dynamic vapor sorption (DVS)

Commercially available DVS equipment (TA instrument, Q5000) was used to obtain adsorption-sorption isotherm of carbonated samples. The samples were soaked in DI water for 48 h before testing to ensure full saturation. After soaking, approximately 15 \sim 20 mg of sample was loaded in a quartz pan. The sample was first equilibrated at 97.5% RH for 5760 s. After this point, the RH was gradually reduced (with 5 \sim 10% RH steps) to obtain the desorption isotherm. After reaching 0% RH, the RH was gradually increased (with 5 to 10% RH steps) up to 97.5% to

obtain adsorption isotherms. Mass equilibrium was reached at each RH when the mass fluctuation was less than 0.001% for 15 min. Throughout the experiment, the temperature was kept constant at 23 $^{\circ}\text{C}.$ During the experiment, N_2 gas was purged.

2.3.8. Scanning electron microscope (SEM)

The microstructures of 14 days and 56 days carbonated cured samples were evaluated using Hitachi 3000 N SEM. The instrument was operated in high vacuum mode with a 30 kV accelerated voltage and a working distance of about 10 mm. The cement paste sample was coated with Platinum (Pt) before capturing the SEM images.

3. Results and discussion

3.1. Mechanical performances

Fig. 1 shows the compressive strength of wollastonite and slag with differing proportions of magnesia for different curing conditions. It can be observed that the addition of magnesia to the wollastonite and slag systems increases the compressive strength significantly. The effects of magnesia on wollastonite after various curing durations are shown in Fig. 1(a). It can be seen that for wollastonite mixes, 25% magnesia incorporation increases the compressive strength by 44%, 19%, and 20% after 14 days, 28 days, and 56 days of the carbonation period, respectively. Fig. 1(b) illustrates the effects of magnesia on slag carbonation. For slag-based mixes, adding 25% magnesia results in an increment of compressive strength by 126%, 121%, and 121%, respectively, for 14 days, 28 days, and 56 days of carbonation curing. Two interesting observations can be drawn from the duration of carbonation curing. Firstly, for early age (14 days) and standard age (28 days) carbonation, it can be observed that the gain in compressive strength is quite rapid and enhanced. In case of wollastonite samples, the addition of 25% magnesia resulted an increase of 37% in compressive strength (14 days to 28 days). Similarly, slag samples with 25% magnesia resulted an increase of 14% in compressive strength (14 days to 28 days). On the other hand, the extended age (56 days) of carbonation curing does not result in a noticeable gain in compressive strength. In case of wollastonite samples, the addition of 25% magnesia resulted an increase of 5% in compressive strength (28 days to 56 days). Similarly, slag samples with 25% magnesia resulted in an increase of 1% in compressive strength (28 days to 56 days). As a result, it can be stated that the maximum gain in compressive strength can be achieved at 28 days of carbonation curing.

The addition of magnesia in a wollastonite and slag system shows an almost similar pattern of compressive strength. It can be seen that 25% incorporation of magnesia results in a gain of compressive strength. On the other hand, incorporation of 50% magnesia results in loss of compressive strength. Magnesia stimulates the production of nesquehonite and hydro-magnesite in wollastonite and slag systems [34]. The formation of nesquehonite and hydro-magnesite can result in the densification of the binder matrix as well as a well-connected network of carbonation products leading to higher load-carrying capacity. Furthermore, a previous study has demonstrated that the elongated morphologies of these magnesium carbonates create a robust interlocking mechanism that enables the development of strength [34]. Moreover, the difference of strength between wollastonite and slag based mixes can be due to different chemical compositions. The higher content of CaO in wollastonite can lead to a slightly higher formation of calcite, causing a denser matrix. On the other hand, it has been reasoned that the continued formation of magnesium carbonates results in the continued expansion of volume, causing rising internal stress. The internal stress leads to macrocrack formation, causing reduced load carrying capacity (Fig. 2).

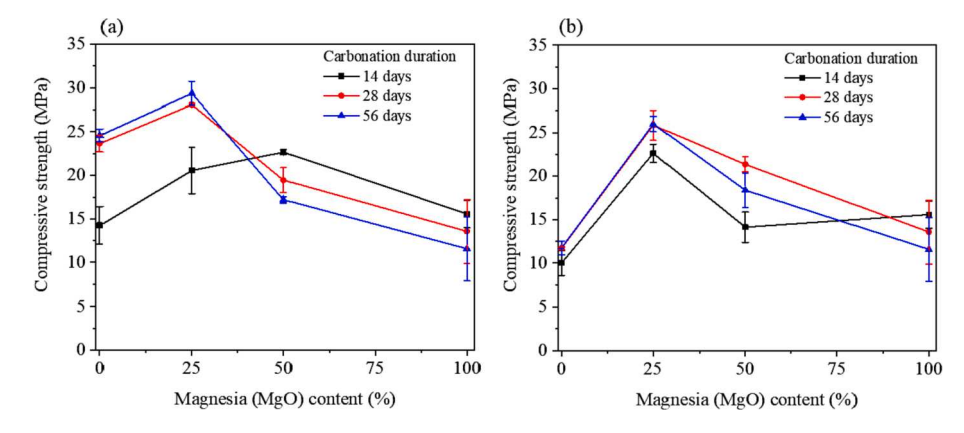


Fig. 1. Compressive strength: Carbonated (a) wollastonite, and (b) slag with different magnesia content.

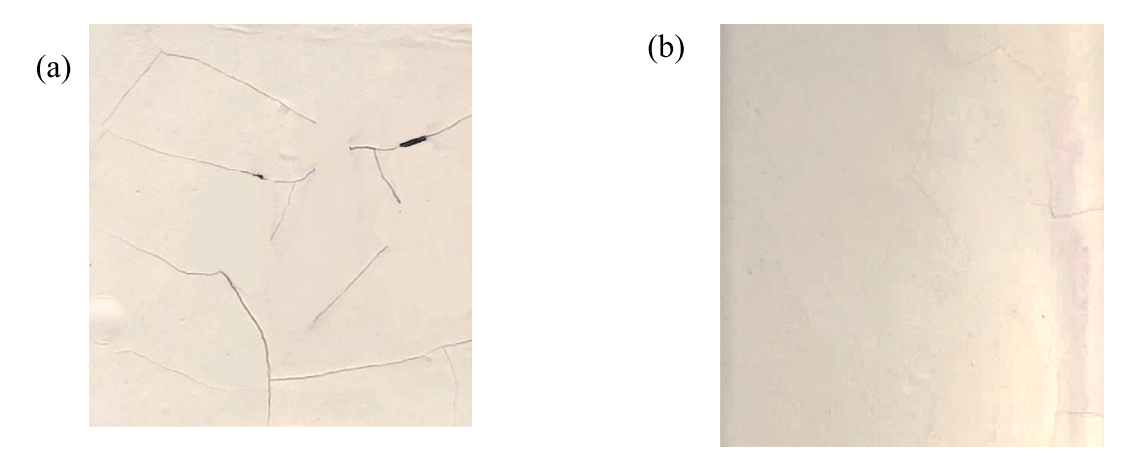


Fig. 2. Macrocracking observed on samples (a) 50% wollastonite- 50% magnesia, and (b) 50% slag-50% magnesia.

3.2. Dimensional stability

Fig. 3 depicts the effects of magnesia on the dimensional change of slag and wollastonite carbonated systems according to the ASTM C157 [33]. It can be observed that introducing magnesia to the carbonated wollastonite and slag system considerably enhances the expansion of length. This is due to the formation of hydrated magnesium carbonate (HMC) during the carbonation in the presence of magnesia. Under carbonation curing, the conversion of $Ca(OH)_2$ to $CaCO_3$ results in an 11.4% increase in solid volume [3]. Whereas, conversion of MgO to Mg

 $(OH)_2$ and $MgCO_3\cdot 3H_2O$ results in an increase of solid volume by 131.4% and 614.3%, respectively [3].

Based on the type of binder, distinct observations can be made from Fig. 3. Fig. 3(a) shows that 25% magnesia addition in carbonated wollastonite system increased length change by 0.025% after 50 days of carbonation curing. However, 50% magnesia addition caused 0.13% length change which is higher than previously reported results [35–37]. On the other hand, 3(b) illustrates 0.06% and 0.12% length expansion for 25% and 50% magnesia addition in carbonated slag composites, respectively. The formation of HMCs have a critical role in the length

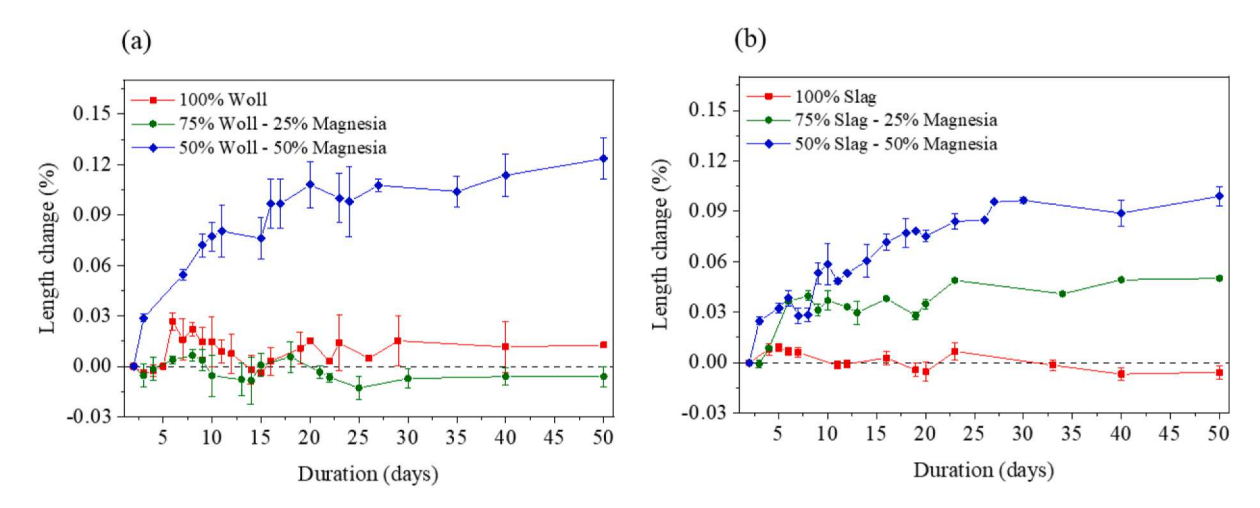


Fig. 3. Length changes with carbonation duration, (a) wollastonite blended with magnesia, (b) slag blended with magnesia. Here Woll represents wollastonite.

change characteristics of carbonated mixes. In case of wollastonite based mixes, on incorporation of 25% magnesia, the length change is lower than that of 100% wollastonite. It can be due to the interlocking of calcite and HMCs, which can provide dimensional stability and restrict the change in length. However, this phenomenon may not exist in slag based mixes due to the lower formation of calcite and higher presence of HMCs. Moreover, in both cases of binder containing 50% magnesia, the higher formation of HMCs occurs. The HMCs have a higher surface area than that of calcite which can lead to increased stress within a closed solid volume. This stress can lead to dimensional instability manifesting in the form of length change. Moreover, as discussed in section 3.1 this dimensional instability coupled with the formation of macro cracks results in reduced strengths.

3.3. Microstructural analysis of carbonated matrix using thermal techniques

Wollastonite and slag react with CO_2 in the presence of water during the carbonation process, producing $CaCO_3$ and Ca-modified silica gel. These two carbonated products contribute towards enhancing mechanical performance and microstructural densification. In case of carbonation of magnesia, the strength gain depends upon the progression of hydration and subsequent carbonation. Magnesia hydrates into brucite $[Mg(OH)_2]$, which is then carbonated, resulting in the formation of HMCs [34]. Most observed HMCs are nesquehonite $(MgCO_3 \cdot 3H_2O)$,

hydro-magnesite [4MgCO $_3$ ·Mg(OH) $_2$ ·4H $_2$ O], and dypingite [4MgCO $_3$ ·Mg(OH) $_2$ ·5H $_2$ O]. The solid and fibrous structures of HMCs results in interlocking between the phases that decreases the initial porosity and provide mechanical strength to the cement-based composites.

Chemically bound water decomposes at temperatures ranging from 100 to $600\,^{\circ}\text{C}$ [38–40]. $\text{Ca}(\text{OH})_2$ decomposes to CaO and H_2O at around $450\,^{\circ}\text{C}$ [38,40,41]. CaCO_3 decomposes to CaO and CO_2 at $600\,^{\circ}\text{C}$ [38,40]. The evaporation of physically absorbed water and bonded water from HMCs can be attributed to the weight loss from 100 to $300\,^{\circ}\text{C}$. The sharp peaks around $370\,^{\circ}\text{C}$ and $390\,^{\circ}\text{C}$ correspond to Mg (OH)₂ dihydroxylation and HMCs decarbonization, respectively [14,15,27,41]. The gradual mass drop from 500 to $600\,^{\circ}\text{C}$ is associated with the decomposition of metastable Ca, Mg-carbonates. Metastable Ca-Mg carbonates are intermediate phases with different ordering patterns such as $\text{Ca}_{0.75}\text{Mg}_{0.23}\text{CO}_3$, $\text{Ca}_{0.67}\text{Mg}_{0.33}\text{CO}_3$ [42].The peak at around $600\,^{\circ}\text{C}$ is due to the decomposition of well-crystallized stable MgCO₃ [15,41,43].

Fig. 4 shows the TGA-MS plots of 14 and 56 days carbonated mixes. Fig. 5 shows the DTG curves of carbonated mixes. It can be seen that increasing the curing time results in increased formation of carbonates in all the binder mixes. This is due to the well established fact that a longer duration of carbonation curing leads to higher $\rm CO_2$ diffusion. This causes amplification in the formation of carbonation products. Furthermore, it should be noted that the effect of carbonation duration is

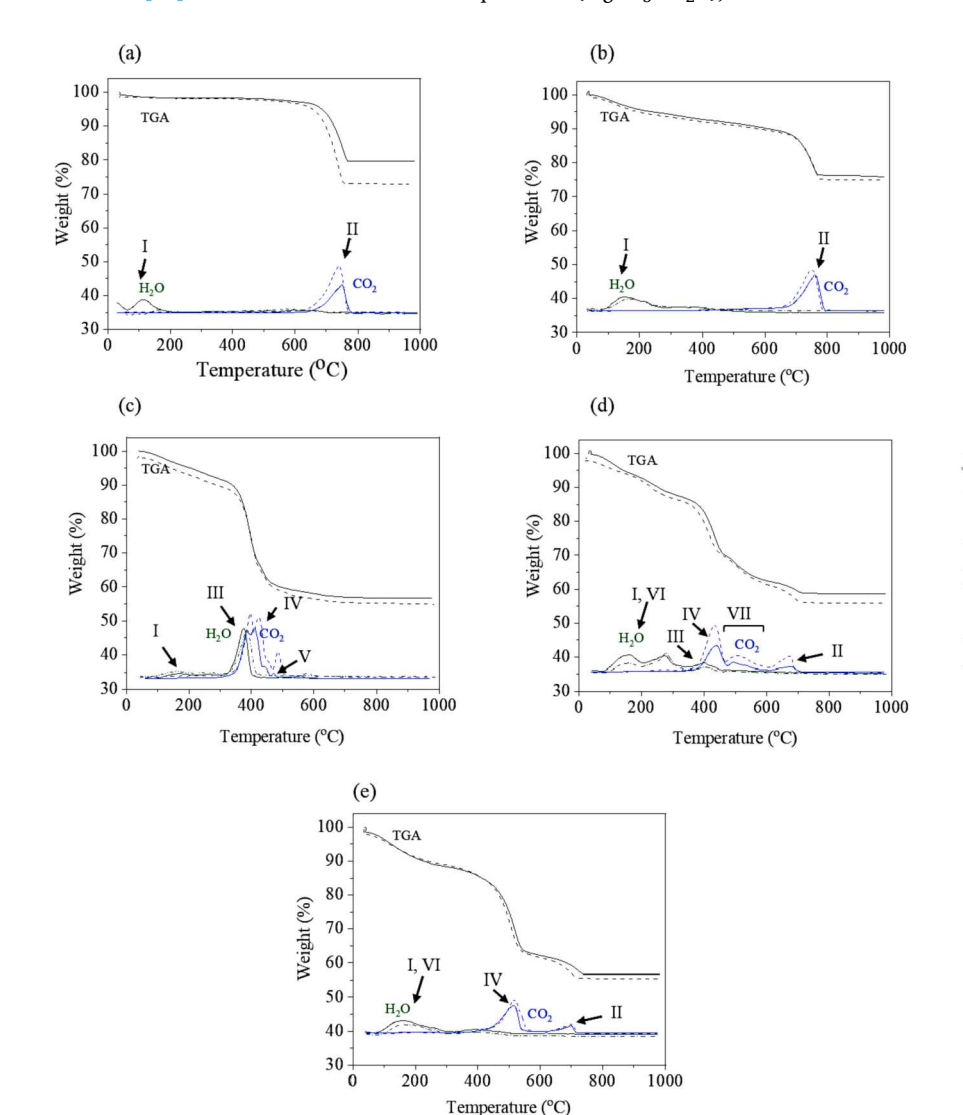


Fig. 4. TGA-MS plots showing the release of H₂O and CO₂ gases from 14 days carbonated matrixes (solid line), and 56 days carbonated matrixes (dashed line): (a) wollastonite, (b) slag, (c) Magnesia, (d) 75% wollastonite-25% Magnesia, (e) 75% slag-25% Magnesia. Here, I: Physically absorbed and chemically bound water, II: Decomposition of CaCO₃, III: Dihydroxylation of Mg(OH)₂, IV: Decarbonization of HMCs, V: Decomposition of stable MgCO₃, VI: Dehydration of HCMs, VII: Decomposition of metastable Ca, Mg-carbonates.

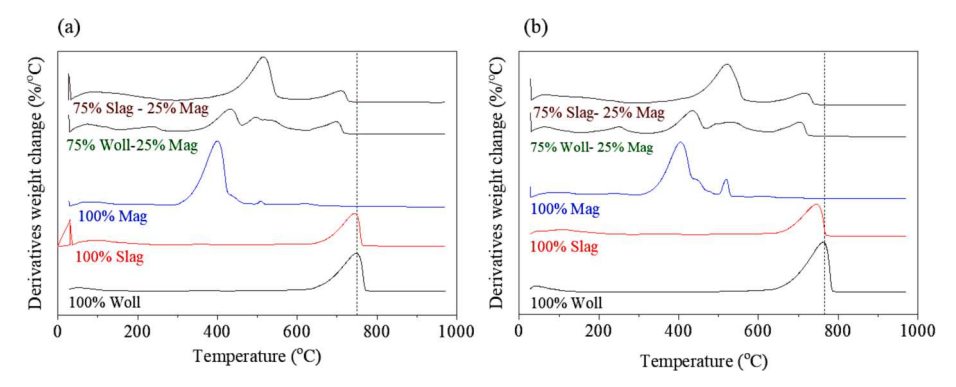


Fig. 5. Derivatives thermogravimetric (DTG) plot, (a) 14 days, (b) 56 days carbonation curing. Here Woll and Mag represent wollastonite and magnesia, respectively.

quite noticeable for 100% magnesia mix. When compared to 14 days the 56 days 100% magnesia mix presents an interesting scenario. For 100% magnesia mixes the longer carbonation curing results in higher formation of HMCs as well magnesium carbonate. This particular phenomenon results in densification of binder matrix. In the case of wollastonite, slag, and magnesia, weight loss below 200 °C is attributed to chemically bound water and physically absorbed water. Wang et al. showed that HMCs were also dehydrated at around 250 °C [15,27]. As illustrated in Fig. 4(c), there was not significant loss of water in case of carbonated magnesia at around 250 °C, which indicates that the HMCs were not dehydrated or were not present in that region. As illustrated in Fig. 4(e), the same thing happened in the slag-magnesia carbonated system. In the slag-magnesia system, HMCs endured very little dehydration, or the presence of HMCs was negligible. However, the higher amount of H₂O has evaporated in wollastonite-magnesia, as seen in Fig. 4(d), indicating the formation of HMCs. There was a gradual weight loss from 400 to 600 °C due to H₂O and CO₂, showing the development of metastable Ca and Mg-carbonates. Fig. 4(a-b) depicts significant weight loss due to CO₂ evaporation at around 750 °C. This weight loss was due to the decomposition of calcite (CaCO₃). As MgCO₃ decomposes before 600 °C, there was no weight loss in the case of carbonated 100% magnesia at this temperature. The gradual weight loss of slag-magnesia and wollastonitemagnesia from 600 to 750 °C was noticed, which denotes the decomposition of metastable CaCO₃ (mCaCO₃) [44].

According to the TGA-MS and DTG plots, metastable $CaCO_3$ along with $MgCO_3$ and HMCs were generated when magnesia was incorporated into slag and wollastonite. In a CO_2 -cured environment, these metastable carbonates and HMCs provides better mechanical properties [20,43]. Furthermore, another important aspect that needs to be discussed here is that a non-hydraulic system wollastonite, when cured under carbonation, can provide a higher amounts of carbonates when compared to a slag mix which is a semi-hydraulic system. Therefore, it can be stated that the classical concept of achieve superior performance and reactivity from semi-hydraulic system compared to that of non-hydraulic system is not true or applicable when carbonation curing of samples is done.

3.4. CO₂ sequestration

Carbonated activated binders, such as slag, wollastonite, and magnesia, are low-carbon cementitious materials due to their ability to sequester CO_2 and improve binding characteristics [27]. Magnesia has a CO_2 sequestration capability of 92.8 wt%, which is more than that of ordinary Portland cement (50.4 wt%) [27]. The present study calculated the carbonated matrix's CO_2 sequestration using thermogravimetric analysis (coupled with mass spectroscopy). Since $\mathrm{Ca}(\mathrm{OH})_2$, $\mathrm{Mg}(\mathrm{OH})_2$, and $\mathrm{Mg}\mathrm{CO}_3$ decompose within a relatively narrow temperature range, calculating CO_2 sequestration from TGA was challenging. As a result, TGA was utilized in conjunction with MS (mass spectroscopy) to identify and quantify the CO_2 gas released from the carbonated matrix.

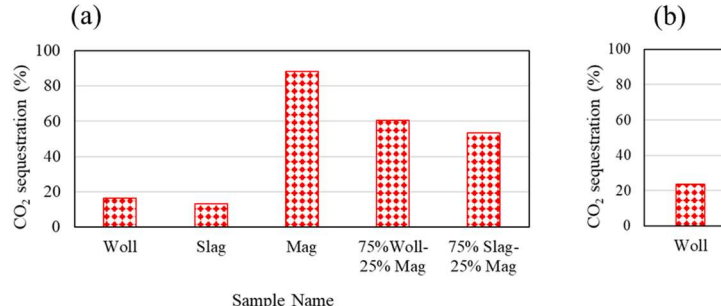
Fig. 6 illustrates the CO_2 sequestration after 14 and 56 days of carbonation curing. Wollastonite, slag, and magnesia sequester 16%, 13%, and 88% (per gram of sample) of CO_2 after 14 days of carbonation curing, respectively. Moreover, the wollastonite-magnesia and slagmagnesia resulted in 60% and 50% CO_2 sequestration, respectively. It can be seen that wollastonite-magnesia sequestered more CO_2 than slagmagnesia. The possibility was that the wollastonite-magnesia system produced more HMCs than the slag-magnesia system (as discussed in section 3.3). After 56 days of carbonation, wollastonite, slag, magnesia, wollastonite-magnesia, and slag-magnesia sequestered 45%, 116%, 7%, 8%, and 5% more CO_2 than after 14 days of carbonation, respectively.

As expected, the 100% magnesia mix presented the highest $\rm CO_2$ sequestration capacity among all the mixes. However, 100% wollastonite and slag mixes presented an interesting observation. For 14 days of carbonation curing 100% wollastonite mix presented higher $\rm CO_2$ sequestration when compared with 100% slag mix. On the other hand, for 56 days of carbonation curing 100% slag mix presented higher $\rm CO_2$ sequestration. It can be due to the formation of carbonates in wollastonite at 14 days which enhances the microstructure but restricts the diffusion of $\rm CO_2$ into the matrix. For 100% slag the low amount of calcium oxide can lead to slow formation of carbonates causing higher $\rm CO_2$ sequestration at later ages. Moreover, the hybrid mixes of wollastonite and slag with magnesia show that incorporating magnesia results in enhanced $\rm CO_2$ sequestration. Based on these findings, it is possible to conclude that incorporating magnesia into a non-hydraulic system result in more significant $\rm CO_2$ sequestration than a semi-hydraulic system.

3.5. Identifying different minerals formed during carbonation reaction using FTIR

From the thermal analysis, CaCO₃, HMCs were detected. Distinct HMCs and different polymorphs of CaCO₃ in the carbonated system could not be distinguished using thermal analysis. The absorbance at around 1420 cm⁻¹ and 872 cm⁻¹ is due to asymmetric stretching vibration (ν_3 mode) and out-of-plane bending (ν_2) of CO₃²⁻ [43], respectively. The broad peak or split peaks at 1420 cm⁻¹ denote amorphous calcium carbonates (ACC), and on the other hand, sharp peaks at 1420 and $872~\text{cm}^{-1}$ denote more stable CaCO_3 , i.e., calcite. Fig. 7 shows the FTIR spectra after 14 days and 56 days of carbonation. In Fig. 7(a), wollastonite shows a broad peak at around 1420 cm⁻¹, which becomes sharper after 56 days of carbonation (Fig. 7(b)). This demonstrates the conversion of ACC to calcite in wollastonite batch due to the prolonged carbonation period. However, peak at 872 cm⁻¹ was present in both cases, indicating calcite formation. An extra aragonite ν_2 bending peak at around $850~\mathrm{cm}^{-1}$ absorbances was observed for slag after 14 days of carbonation curing. For 14 days of carbonation and 56 days of carbonation, the spectra of slag did not showed any significant changes. As a result, it can be stated that no mineralogical change occurred after 14 days of carbonation in the case of slag.

The absorbance peaks at 1423 and 1484 cm⁻¹ are attributed to



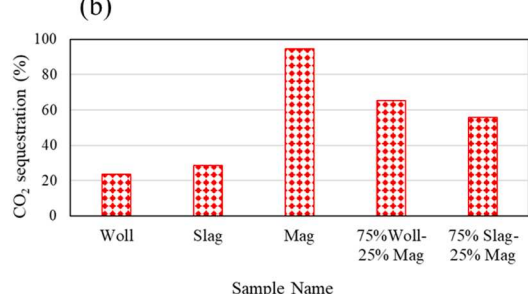


Fig. 6. CO₂ sequestration after, (a) 14 days, (b) 56 days carbonation. Here Woll and Mag represent wollastonite and magnesia, respectively.

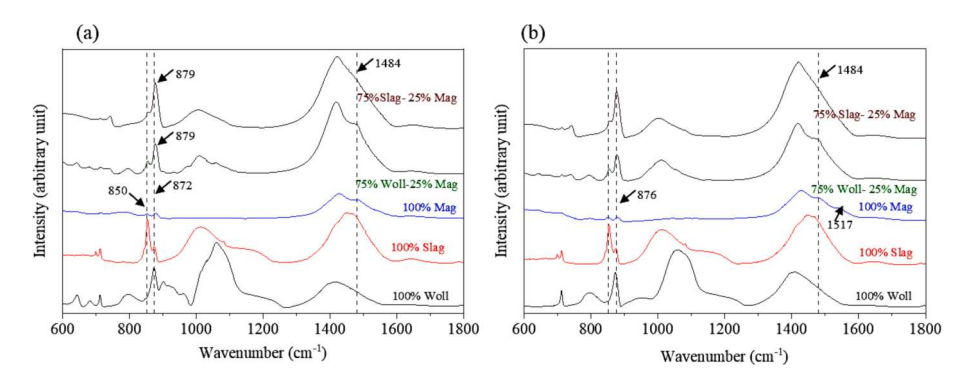


Fig. 7. FTIR spectra of (a) 14 days, (b) 56 days of carbonation cured samples. Here Woll and Mag represent wollastonite and magnesia, respectively.

antisymmetric stretching vibration (ν_3 mode) of hydro-magnesite [15,24,45,46], whereas the shoulder at 1517 cm $^{-1}$ is due to nesquehonite [15,24]. The low-intensity band at 850 and 880 cm $^{-1}$ correspond to the bending vibration of CO₃, represents the formation of hydro-magnesites [43,46]. Fourteen days of carbonated magnesia contains 1423, 1484, 850, 879 cm $^{-1}$ peaks of hydro-magnesite. The 1517 cm $^{-1}$ peak for nesquehonite was only present for 56 days of carbonated magnesia.

It can be seen that the duration of carbonation curing has a minor role in the formation of polymorphs. The only variable having a significant influence on carbonation products is the amount of magnesia in hybrid mixes. The incorporation of magnesia shows aragonite and hydro-magnesite absorbance peaks at 850 cm⁻¹. In a carbonated environment, the coexistence of wollastonite and magnesia may result in the formation of aragonite or hydro-magnesite. The 850 cm⁻¹ peak was of quite lower intensity in the slag-magnesia carbonated system than in the carbonated slag system. Furthermore, 1484 cm⁻¹ hydro-magnesite peak was prominent for the wollastonite-magnesia system but was absent or merged with CaCO₃ peaks for the slag-magnesia carbonated system. This shows that little or no hydro-magnesite was present in the slag-magnesia system. The 1517 cm⁻¹ absorbance peak of nesquehonite was absent in the slag-magnesia and wollastonite-magnesia system after 56 days of carbonation. It is worth noting that after 56 days of carbonation, the absorbance peak at $879\,\mbox{cm}^{-1}$ merges with the calcite peak and form the peak at 876 cm^{-1} .

It should be noted that the 100% wollastonite and slag both have different forms carbonates. As seen in Fig. 7 the calcite peak is observed in wollastonite mix, whereas slag mix spectra show aragonite peak. On the other hand, when magnesia is introduced into the slag system, the peak shift shows the formation of calcite. Moreover, the wollastonite and magnesia mix shows the presence of both calcite and aragonite. As discussed previously, it is possible to conclude that the generation of hydro-magnesite is more significant in non-hydraulic carbonated systems than in semi-hydraulic systems.

3.6. X-ray diffraction analysis

Fig. 8 illustrates the XRD pattern of 14 days and 56 days of carbonated wollastonite, slag, magnesia, wollastonite-magnesia, slag-magnesia, respectively. Carbonated wollastonite mostly has unreacted wollastonite and calcite phases. Carbonated slag mostly has aragonite and calcite in the system. Formation of vaterite was also seen in slag mix system. Carbonated magnesia has mostly brucite $(Mg(OH)_2)$ and magnesite $(MgCO_3)$. Hydro-magnesite and nesquehonite with minimal intensity were also observed.

When magnesia and wollastonite were combined, the formation of calcite and magnesite drastically decreased. Polymorphs of calcite namely, aragonite and vaterite were found in the carbonated wollastonite-magnesia mix. In the case of the slag-magnesia carbonated system, the formation of calcite reduced significantly. Magnesite was also formed in the slag-magnesia mix.

An interesting observation is the consumption of brucite in the wollastonite and slag mixes. Although the amount of magnesia (25%) is quite reduced in the wollastonite and slag based mixes. The brucite was consumed to form HMCs in the wollastonite and slag mixes. It should be noted that magnesia was included into both slag and wollastonite, however, the carbonation products in both the binder matrix differ widely from each other. In case of slag-magnesia system magnesite was the dominating phase whereas in case of wollastonite-magnesia system presented hydro-magnesite phase along with calcite. It can be stated that both semi and non-hydraulic binder have different behavior when magnesia is introduced into the matrix.

3.7. Pore structure analysis using dynamic vapor sorption

Vapor sorption analysis is usually performed to characterize gel phases (C-S-H or Ca-modified silica gel). Due to the smaller molecule size of water compared to that of nitrogen or mercury, vapor sorption analysis is more beneficial to analyze the nano porosity than other traditional techniques (i.e., MIP or nitrogen sorption)[32]. A typical plot

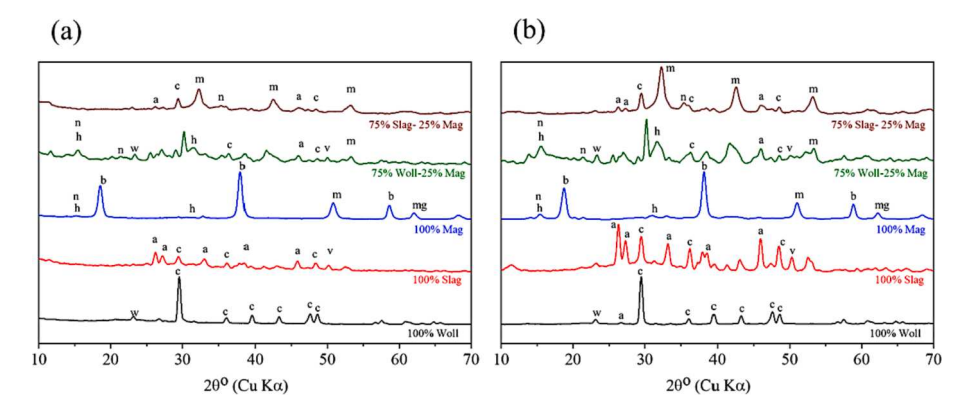


Fig. 8. XRD plots of carbonated matrix after (a) 14 days, and (b) 56 days of carbonation. Here, a: aragonite, b: brucite, c: calcite, h: hydro-magnesite, m; magnesite, mg; magnesia, n: nesquehonite, v: vaterite w: wollastonite.

of the hysteresis loop of desorption and adsorption isotherm is shown in Fig. 9(a). The hysteresis loop between adsorption and desorption is found in all the matrixes, and they contribute to the complex nature of pore connectivity [47,48]. The matrixes' specific surface area was determined using the BET method [49]. Pore size distribution was determined using the BJH (Barrett, Joyner, and Halenda) model incorporating the statical water layer thickness proposed by Hagymassy [50,51].

The specific surface area of the carbonated matrix is shown in Fig. 9 (b). It can be observed that carbonated wollastonite has a higher surface area (85.3 $\rm m^2/g)$ than carbonated slag (33.4 $\rm m^2/g)$ and magnesia (44.7 $\rm m^2/g)$). However, the inclusion of magnesia in slag and wollastonite yielded 74 $\rm m^2/g$ and 84.1 $\rm m^2/g$ specific surface area, respectively. This indicates that higher crystalline carbonated products were formed when magnesia was added to the slag and wollastonite systems.

Fig. 10 shows the pore size distribution of the carbonated matrixes. Carbonated wollastonite and slag show a significant peak before 1 nm and another at around 1.5 nm. On the other hand, carbonated magnesia shows three peaks, i.e., before 1 nm, 1.5 nm, and 3 nm. However, when magnesia was added with wollastonite or slag, all the peaks merged into one prominent peak before 1 nm. This shows that when magnesia was added with slag and wollastonite, the higher formation of carbonated products reduces the large pore size.

Based on the previous study, the pores in the carbonated matrix can be divided in the following groups (based on the pore diameter), (i) inter-cluster spaces (diameter: less than 2 nm), (ii) gel pores (diameter: 2–10 nm), (iii) capillary pores (diameter: 10–41 nm) [32,52]. The pore diameter below 2 nm is assumed to contain physiosorbed and

chemisorbed water within an outer layer of Ca-modified silica gel clusters [32]. From Fig. 11, it can be observed that carbonated wollastonite has a minimum volume of capillary pores, and carbonated magnesia has a maximum volume of capillary pores. Carbonated wollastonite-magnesia contains the highest volume of inter-particle porosity, and carbonated magnesia has a minimum volume of interparticle porosity.

From the pore structure investigation, it can be observed that the incorporation of magnesia leads to a pore size refinement. This can be attributed to the formation of HMCs along with carbonated products which can lead to densification of matrix. However, as seen in Fig. 11 the pore volume of hybrid mixes in both wollastonite and slag mixes are higher than that of 100% wollastonite and slag mix.

3.8. Carbonate morphologies

Fig. 12 and Fig. 13 reveal the microstructures of wollastonite, slag, and magnesia subjected to carbonation curing for 14 and 56 days. As shown in Fig. 12(a-d) calcite was observed in both carbonated wollastonite and slag. The abundance of calcite in the wollastonite mix (Fig. 12 (a-b)) illustrates the higher reactivity of wollastonite to carbonation when compared to slag. However, it should be noted that when comparing the 14 days carbonated slag, the wollastonite mix showed a denser microstructure. This phenomenon can lead to difficulty of $\rm CO_2$ penetration at later ages of curing which was also discussed in section 3.4. Furthermore, the wollastonite matrix contained no mCaCO $_3$ which shows its higher carbonation reactivity. Aragonite with its distinct morphology was also observed in slag mixes at 14 days which later gets

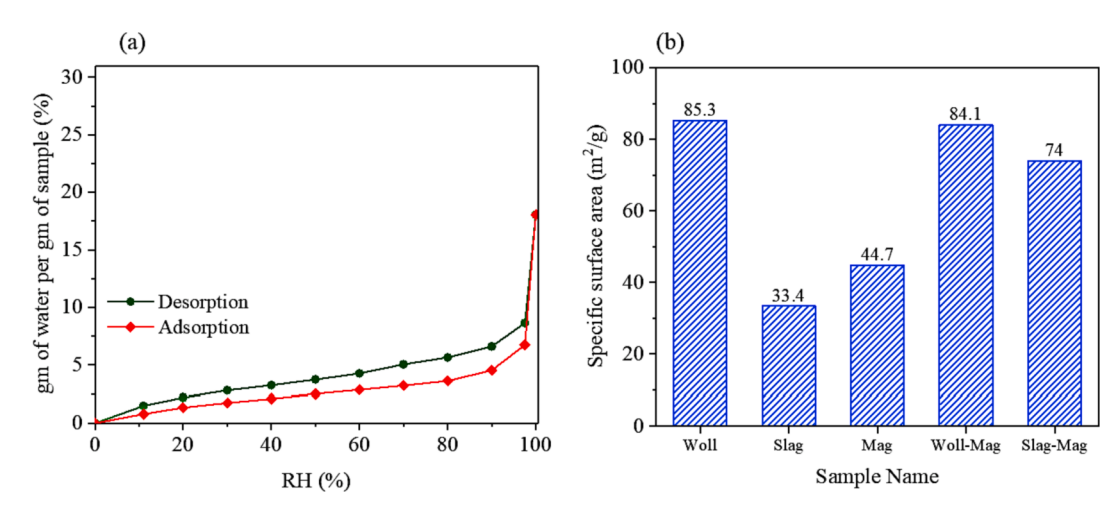


Fig. 9. (a) A typical plot of vapor desorption and adsorption curves for wollastonite-magnesia carbonated matrix, (b) specific surface area (S_{BET}) of 14 days of carbonated matrixes. Here Woll and Mag represent wollastonite and magnesia, respectively.

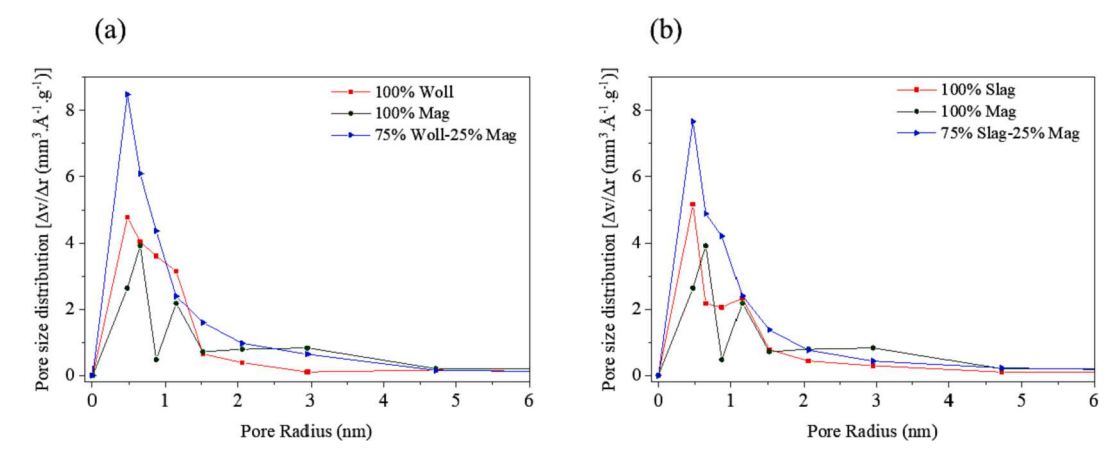


Fig. 10. Pore size distribution of 14 days carbonated matrixes: (a) wollastonite-magnesia, (b) slag-magnesia. Here Woll and Mag represent wollastonite and magnesia, respectively.

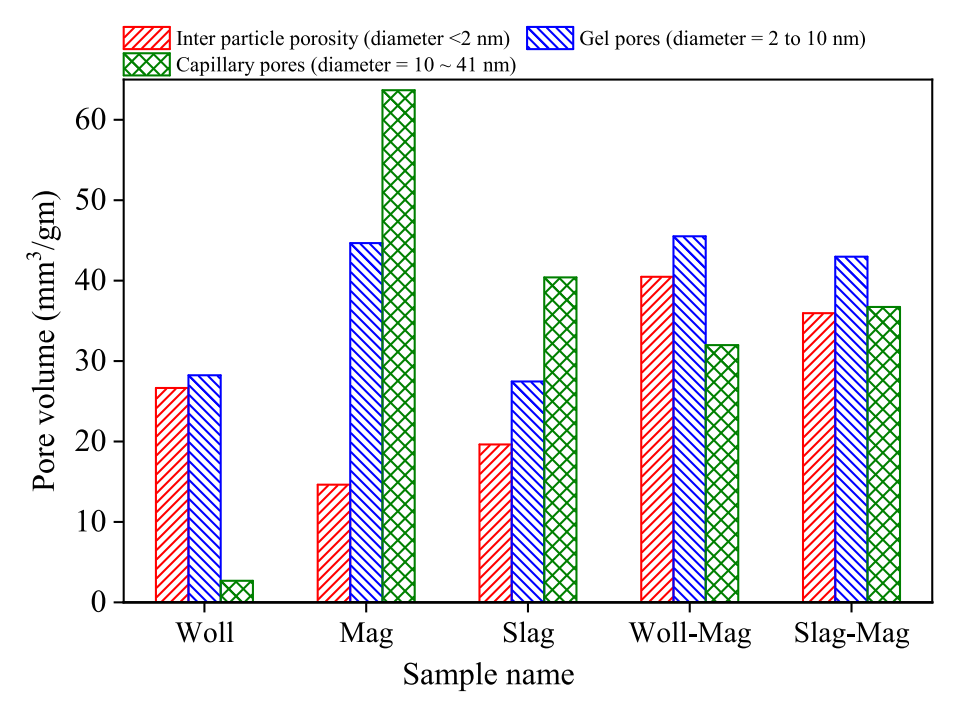


Fig. 11. Pore size distribution of 14 days of carbonated matrixes. Here Woll and Mag represent wollastonite and magnesia, respectively.

transformed to stable calcite crystal. For carbonation cured magnesia, mostly magnesite was found. Since the entire area is covered with magnesite at both the ages of curing it can be stated that the formation of magnesite can lead to densification of microstructure.

The hybrid mixes of wollastonite and slag showed the presence of hydro-magnesite. However, a stark difference in both the mixes morphology can also be observed. For wollastonite-magnesia mixes at 14 and 56 days, the wollastonite was covered in metastable ${\rm CaCO_3}$. Moreover, the formation of hydro-magnesite was also enhanced when the curing duration was increased from 14 to 56 days. This can lead to the macrocracking of the surface, causing lower compressive strength. On the contrary, slag-magnesia based mixes showed amorphous ${\rm CaCO_3}$ along with hydro-magnesite. This morphology will also lead to matrix densification but will have a reduced effect on macrocracking. The morphology of hybrid mixes further concurs the fact that wollastonite, a non-hydraulic system, has higher reaction activity to carbonation than slag, a semi-hydraulic system.

4. Conclusion

In this study, carbonation products of wollastonite, slag and magnesia mixes were investigated by various techniques, including compressive strength, TGA-MS, XRD, FTIR, DVS and SEM. The following concluding points can be drawn from the findings,

- (i) The addition of magnesia in carbonated calcium silicates (either slag or wollastonite) increases the composites' compressive strength by more than 44% for wollastonite, and 126% for slag, respectively (for 14 days of curing). Such a drastic increase in the mechanical performances of the composites was attributed to the pore size refinement due to the addition of magnesia.
- (ii) The magnesia dosage can significantly affect the carbonate phases formed in the CO₂ cured cementitious composites. Specifically, it was found that the addition of 25% magnesia to carbonated wollastonite and slag composites enhanced the development of HMCs while also modified the CaCO₃ polymorphs in the wollastonite carbonated system.

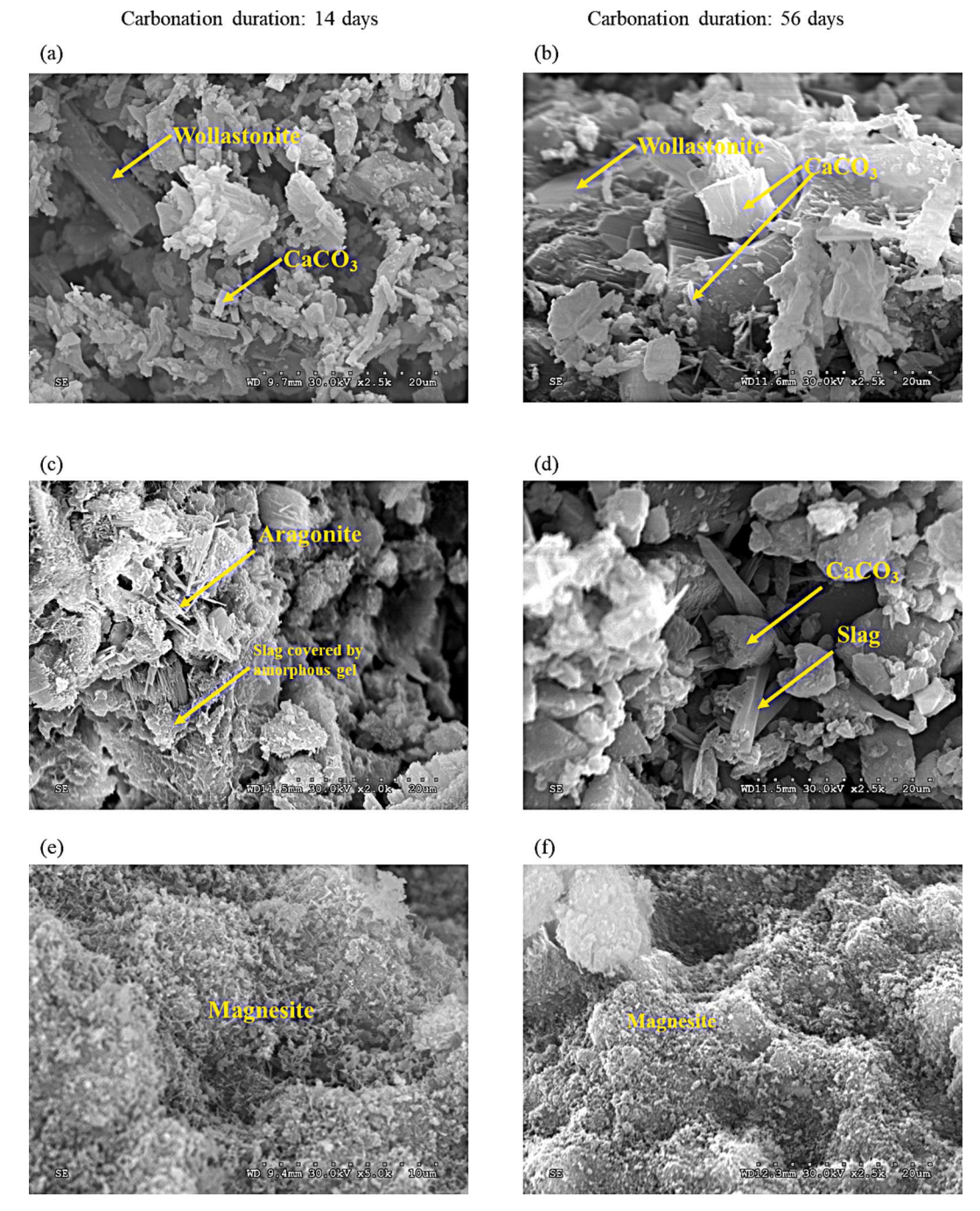


Fig. 12. SEM images of carbonated matrixes, (a-b) wollastonite, (c-d) slag, (e-f) magnesia.

- (iii) Formation of HMCs in carbonated composites was found to refine the pore size distribution by reducing the critical pore diameter. The relative amounts of nano-porosity were also higher in slagmagnesia and wollastonite-magnesia binary systems compared to those present in a single type of binder.
- (iv) The addition of magnesia was observed to increase the expansion of the carbonated composites produced using either slag or wollastonite. The increase in the dosage of magnesia also increased the expansion. Such expansion of the composites was expected due to the formation of expansive HMCs in these matrixes. The maximum expansion of the samples remained below 0.1% for the tested duration for 25% magnesia addition.

The most interesting finding of this study is that for carbonation

cured calcium silicate composites, while the addition of magnesia offers a potential pathway to significantly improve the performance of both semi-hydraulic and non-hydraulic systems, the benefits were more pronounced in the case of non-hydraulic system.

CRediT authorship contribution statement

Rakibul I. Khan: Conceptualization, Data curation, Formal analysis, Investigation, Writing – original draft. Salman Siddique: Conceptualization, Investigation, Writing – review & editing. Warda Ashraf: Conceptualization, Formal analysis, Investigation, Funding acquisition, Supervision, Writing – review & editing.

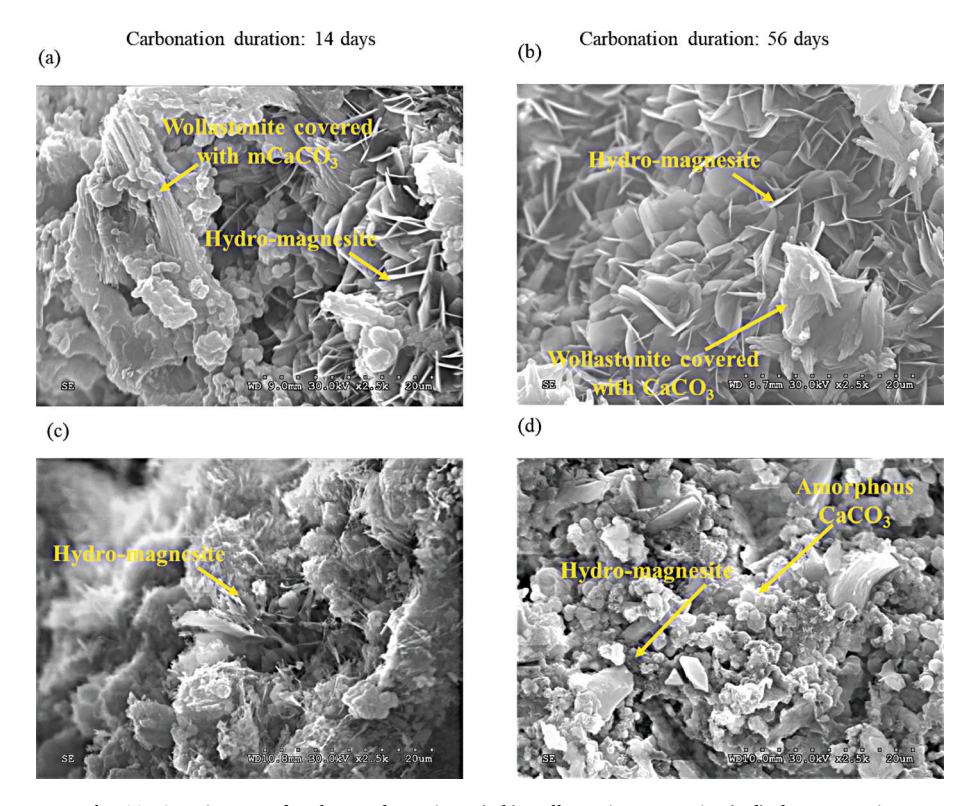


Fig. 13. SEM images of carbonated matrixes: (a-b) wollastonite-magnesia, (c-d) slag-magnesia.

Declaration of Competing Interest

The authors declare that they have no known competing financial interests or personal relationships that could have appeared to influence the work reported in this paper.

Acknowledgement

This work was conducted with partial funding support from the US National Science Foundation (NSF # ECI - 2028462), Defense Advanced Research Projects Agency (DARPA #W911NF2010308)- Young Faculty Award for Dr. Warda Ashraf. All opinions, findings, and conclusions or recommendations expressed in this material are those of the authors and do not necessarily reflect the views of the funding agencies. The TGA-MS measurements were collected using the IMSERC facilities at Northwestern University, which has received support from the Soft and Hybrid Nanotechnology Experimental (SHyNE) Resource (NSF ECCS-1542205), the State of Illinois, and the International Institute for Nanotechnology (IIN).

References

- [1] M.Á. Sanjuán, E. Estévez, C. Argiz, D. del Barrio, Effect of curing time on granulated blast-furnace slag cement mortars carbonation, Cem. Concr. Compos. 90 (2018) 257–265, https://doi.org/10.1016/j.cemconcomp.2018.04.006.
- [2] S. Ahmad, R.A. Assaggaf, M. Maslehuddin, O.S.B. Al-Amoudi, S.K. Adekunle, S. I. Ali, Effects of carbonation pressure and duration on strength evolution of concrete subjected to accelerated carbonation curing, Constr. Build. Mater. 136 (2012) 565–573. https://doi.org/10.1016/j.conbuildmat.2017.01.069
- [3] L. Mo, D.K. Panesar, Accelerated carbonation A potential approach to sequester CO2 in cement paste containing slag and reactive MgO, Cem. Concr. Compos. 43 (2013) 69–77, https://doi.org/10.1016/j.cemconcomp.2013.07.001.
- [4] K. Mandel, H. Funke, M. Lindner, S. Gelbrich, L. Kroll, T. Schwarz, Recipe development of low-cost wollastonite-based phosphate cements, Constr. Build. Mater. 189 (2018) 86–94, https://doi.org/10.1016/j.conbuildmat.2018.08.207.
- [5] W.J.J. Huijgen, G.J. Witkamp, R.N.J. Comans, Mechanisms of aqueous wollastonite carbonation as a possible CO2 sequestration process, Chem. Eng. Sci. 61 (2006) 4242–4251, https://doi.org/10.1016/j.ces.2006.01.048.
- [6] D. Daval, I. Martinez, J. Corvisier, N. Findling, B. Goffé, F. Guyot, Carbonation of Ca-bearing silicates, the case of wollastonite: Experimental investigations and

- kinetic modeling, Chem. Geol. (2009), https://doi.org/10.1016/j.chemgeo.2009.01.022.
- [7] M. Abdel Wahab, I. Abdel Latif, M. Kohail, A. Almasry, The use of Wollastonite to enhance the mechanical properties of mortar mixes, Constr. Build. Mater. 152 (2017) 304–309, https://doi.org/10.1016/j.conbuildmat.2017.07.005.
- [8] Z. He, A. Shen, Z. Lyu, Y. Li, H. Wu, W. Wang, Effect of wollastonite microfibers as cement replacement on the properties of cementitious composites: A review, Constr. Build. Mater. 261 (2020), 119920, https://doi.org/10.1016/j. conbuildmat.2020.119920.
- [9] L. Wang, S.S. Chen, D.C.W. Tsang, C.S. Poon, K. Shih, Recycling contaminated wood into eco-friendly particleboard using green cement and carbon dioxide curing, J. Clean. Prod. 137 (2016) 861–870, https://doi.org/10.1016/j. iclepro.2016.07.180.
- [10] L.J. Vandeperre, M. Liska, A. Al-Tabbaa, Hydration and mechanical properties of magnesia, pulverized fuel ash, and portland cement blends, J. Mater. Civ. Eng. 20 (2008) 375–383, https://doi.org/10.1061/(asce)0899-1561(2008)20:5(375).
- [11] S.A. Walling, J.L. Provis, Magnesia-based cements: A journey of 150 years, and cements for the future? Chem. Rev. 116 (2016) 4170–4204, https://doi.org/ 10.1021/acs.chemrev.5b00463.
- [12] L.J. Vandeperre, M. Liska, A. Al-Tabbaa, Microstructures of reactive magnesia cement blends, Cem. Concr. Compos. 30 (2008) 706–714, https://doi.org/ 10.1016/j.cemconcomp.2008.05.002.
- [13] C. Unluer, A. Al-Tabbaa, Enhancing the carbonation of MgO cement porous blocks through improved curing conditions, Cem. Concr. Res. 59 (2014) 55–65, https:// doi.org/10.1016/j.cemconres.2014.02.005.
- [14] R. Zhang, N. Bassim, D.K. Panesar, Characterization of Mg components in reactive MgO - Portland cement blends during hydration and carbonation, J. CO2 Util. 27 (2018) 518–527, https://doi.org/10.1016/j.jcou.2018.08.025.
- [15] N.T. Dung, R. Hay, A. Lesimple, K. Celik, C. Unluer, Influence of CO2 concentration on the performance of MgO cement mixes, Cem. Concr. Compos. 115 (2021), https://doi.org/10.1016/j.cemconcomp.2020.103826.
- [16] J.J. Thomas, S. Musso, I. Prestini, T. Troczynski, Kinetics and activation energy of magnesium oxide hydration, J. Am. Ceram. Soc. 97 (1) (2014) 275–282.
- [17] C. Unluer, A. Al-Tabbaa, The role of brucite, ground granulated blastfurnace slag, and magnesium silicates in the carbonation and performance of MgO cements, Constr. Build. Mater. 94 (2015) 629–643, https://doi.org/10.1016/j. conbuildmat.2015.07.105.
- [18] N.K. Lee, K.T. Koh, M.O. Kim, G.H. An, G.S. Ryu, Physicochemical changes caused by reactive MgO in alkali-activated fly ash/slag blends under accelerated carbonation, Ceram. Int. 43 (2017) 12490–12496, https://doi.org/10.1016/j. ceramint.2017.06.119.
- [19] F. Jin, K. Gu, A. Al-Tabbaa, Strength and hydration properties of reactive MgOactivated ground granulated blastfurnace slag paste, Cem. Concr. Compos. 57 (2015) 8–16. https://doi.org/10.1016/j.cemconcomp.2014.10.007.
- [20] G. Mármol, L. Mattoso, A.C. Correa, C.A. Fioroni, H. Savastano, Influence of cellulose pulp on the hydration followed by fast carbonation of MgO-based binders, J. CO2 Util. 41 (2020), https://doi.org/10.1016/j.jcou.2020.101236.

- [21] P. Ballirano, C. De Vito, V. Ferrini, S. Mignardi, The thermal behaviour and structural stability of nesquehonite, MgCO3·3H2O, evaluated by in situ laboratory parallel-beam X-ray powder diffraction: New constraints on CO2 sequestration within minerals, J. Hazard. Mater. 178 (2010) 522–528, https://doi.org/10.1016/ j.jhazmat.2010.01.113.
- [22] M. Merlini, F. Sapelli, P. Fumagalli, G.D. Gatta, P. Lotti, S. Tumiati, M. Aabdellatief, A. Lausi, J. Plaisier, M. Hanfland, W. Crichton, J. Chantel, J. Guignard, C. Meneghini, A. Pavese, S. Poli, High-temperature and high-pressure behavior of carbonates in the ternary diagram CaCO3-MgCO3-FeCO3, Am. Mineral. 101 (2016) 1423–1430, https://doi.org/10.2138/am-2016-5458.
- [23] W. Cheng, C. Zhang, H. Cheng, Z. Chen, H. Liao, F. Cheng, Effect of ethanol on the crystallization and phase transformation of MgCO3·3H2O in a MgCl2-CO2-NH3·H2O system, Powder Technol. 335 (2018) 164–170, https://doi. org/10.1016/j.powtec.2018.04.063.
- [24] V. Ferrini, C. De Vito, S. Mignardi, Synthesis of nesquehonite by reaction of gaseous CO2 with Mg chloride solution: Its potential role in the sequestration of carbon dioxide, J. Hazard. Mater. 168 (2009) 832–837, https://doi.org/10.1016/j. ibazmat 2009.02.103
- [25] S. Gerdemann, D. Dahlin, W. Oconnor, Carbon Dioxide Sequestration by Aqueous Mineral Carbonation of Magnesium Silicate Minerals, Greenh. Gas Control Technol. - 6th Int. Conf. (2003) 677–682, https://doi.org/10.1016/b978-008044276-1/50108-2.
- [26] H.L. Wu, D. Zhang, B.R. Ellis, V.C. Li, Development of reactive MgO-based Engineered Cementitious Composite (ECC) through accelerated carbonation curing, Constr. Build. Mater. 191 (2018) 23–31, https://doi.org/10.1016/j. conbuildmat.2018.09.196.
- [27] L. Wang, L. Chen, J.L. Provis, D.C.W. Tsang, C.S. Poon, Accelerated carbonation of reactive MgO and Portland cement blends under flowing CO2 gas, Cem. Concr. Compos. 106 (2020), https://doi.org/10.1016/j.cemconcomp.2019.103489.
- [28] L. Pu, C. Unluer, Durability of carbonated MgO concrete containing fly ash and ground granulated blast-furnace slag, Constr. Build. Mater. 192 (2018) 403–415, https://doi.org/10.1016/j.conbuildmat.2018.10.121.
- [29] S.A. Bernal, R. San Nicolas, R.J. Myers, R. Mejía De Gutiérrez, F. Puertas, J.S.J. Van Deventer, J.L. Provis, MgO content of slag controls phase evolution and structural changes induced by accelerated carbonation in alkali-activated binders, Cem. Concr. Res. 57 (2014) 33–43, https://doi.org/10.1016/j.cemconres.2013.12.003.
- [30] W. Ashraf, J. Olek, Carbonation behavior of hydraulic and non-hydraulic calcium silicates: potential of utilizing low-lime calcium silicates in cement-based materials, J. Mater. Sci. 51 (2016) 6173–6191, https://doi.org/10.1007/s10853-016-9909-4.
- [31] K. Svensson, A. Neumann, F. Feitosa Menezes, C. Lempp, H. Pöllmann, Carbonation of natural pure and impure wollastonite, SN, Appl. Sci. 1 (2019) 1–12, https://doi. org/10.1007/s42452-019-0328-4.
- [32] W. Ashraf, J. Olek, Elucidating the accelerated carbonation products of calcium silicates using multi-technique approach, J. CO2 Util. 23 (2018) 61–74, https://doi.org/10.1016/j.jcou.2017.11.003.
- [33] ASTM:C157/C157M-08, Standard Test Method for Length Change of Hardened Hydraulic-Cement Mortar and Concrete, ASTM Int. 08 (2008) 1–7. 10.1520/ C0157
- [34] L. Pu, C. Unluer, Performance and microstructure of carbonated MgO samples under high temperatures, J. Mater. Civ. Eng. 31 (2019) 1–9, https://doi.org/ 10.1061/(ASCE)MT.1943-5533.0002624.
- [35] M.S. Eisa, M.E. Basiouny, E.A. Fahmy, Effect of metakaolin-based geopolymer concrete on the length of rigid pavement slabs, Innov. Infrastruct. Solut. 6 (2021) 1–9, https://doi.org/10.1007/s41062-021-00465-5.

- [36] M. Hsie, C. Tu, P.S. Song, Mechanical properties of polypropylene hybrid fiber-reinforced concrete, Mater. Sci. Eng. A. 494 (2008) 153–157, https://doi.org/10.1016/j.msea.2008.05.037.
- [37] N.S. Folliard, J. Kevin, Berke, Properties of high-performance concrete containing shrinkage-reducing admixture, Angew. Chem. Int. Ed. 6(11), 951–952. 27 (1967) 1357–1364. doi.org/10.1016/S0008-8846(97)00135-X.
- [38] G. Villain, M. Thiery, G. Platret, Measurement methods of carbonation profiles in concrete: Thermogravimetry, chemical analysis and gammadensimetry, Cem. Concr. Res. 37 (2007) 1182–1192, https://doi.org/10.1016/j. cemconres.2007.04.015.
- [39] W. Deboucha, N. Leklou, A. Khelidj, M.N. Oudjit, Hydration development of mineral additives blended cement using thermogravimetric analysis (TGA): Methodology of calculating the degree of hydration, Constr. Build. Mater. 146 (2017) 687–701, https://doi.org/10.1016/j.conbuildmat.2017.04.132.
- [40] K. Scrivener, R. Snellings, B. Lothenbach, A Practical Guide to Microstructural Analysis of Cementitious Materials, 2018. 10.1201/b19074.
- [41] L. Mo, D.K. Panesar, Effects of accelerated carbonation on the microstructure of Portland cement pastes containing reactive MgO, Cem. Concr. Res. 42 (2012) 769–777, https://doi.org/10.1016/j.cemconres.2012.02.017.
- [42] P.E. Rosenberg, Synthesis of metastable Ca'Mg carbonates, Am. Mineral. 72 (1987) 1239–1240. https://pubs.geoscienceworld.org/msa/ammin/article-abstract/72 /11-12/1239/41982/Synthesis-of-metastable-Ca-Mg-carbonates?redirectedFr om=fulltext.
- [43] N.T. Dung, C. Unluer, Carbonated MgO concrete with improved performance: The influence of temperature and hydration agent on hydration, carbonation and strength gain, Cem. Concr. Compos. 82 (2017) 152–164, https://doi.org/10.1016/ j.cemconcomp.2017.06.006.
- [44] R.I. Khan, W. Ashraf, J. Olek, Amino acids as performance-controlling additives in carbonation-activated cementitious materials, Cem. Concr. Res. 147 (2021) 1–39, https://doi.org/10.1016/j.cemconres.2021.106501.
- [45] L. Hopkinson, K. Rutt, G. Cressey, The transformation of nesquehonite to hydromagnesite in the system CaO-MgO-H2O-CO2: An experimental spectroscopic study, J. Geol. 116 (2008) 387–400, https://doi.org/10.1086/588834.
- [46] R. Hay, N.T. Dung, A. Lesimple, C. Unluer, K. Celik, Mechanical and microstructural changes in reactive magnesium oxide cement-based concrete mixes subjected to high temperatures, Cem. Concr. Compos. 118 (2021), 103955, https://doi.org/10.1016/j.cemconcomp.2021.103955.
- [47] A. Kumar, S. Ketel, K. Vance, T. Oey, N. Neithalath, G. Sant, Water vapor sorption in cementitious materials-measurement, modeling and interpretation, Transp. Porous Media. 103 (2014) 69–98, https://doi.org/10.1007/s11242-014-0288-5.
- [48] M.B. Pinson, T. Zhou, H.M. Jennings, M.Z. Bazant, Inferring pore connectivity from sorption hysteresis in multiscale porous media, J. Colloid Interface Sci. 532 (2018) 118–127, https://doi.org/10.1016/j.jcis.2018.07.095.
- [49] S. Brunauer, P.H. Emmett, E. Teller, Adsorption of gases in multimolecular layers, J. Am. Chem. Soc. 60 (2) (1938) 309–319.
- [50] P.P. Barrett, Elliott; Joyner, Leslei G; Halenda, The determination of pore volume and area distributions in porous substances. I. Computations from nitrogen isotherms, (1951).
- [51] J. Hagymassy, S. Brunauer, R.S. Mikhail, Pore structure analysis by water vapor adsorption. I. t-Curves for water vapor, J. Colloid Interface Sci. 29 (3) (1969) 485–491.
- [52] H.M. Jennings, A. Kumar, G. Sant, Quantitative discrimination of the nano-pore-structure of cement paste during drying: New insights from water sorption isotherms, Cem. Concr. Res. 76 (2015) 27–36, https://doi.org/10.1016/j.cemconres.2015.05.006.